



저작자표시-비영리-변경금지 2.0 대한민국

이용자는 아래의 조건을 따르는 경우에 한하여 자유롭게

- 이 저작물을 복제, 배포, 전송, 전시, 공연 및 방송할 수 있습니다.

다음과 같은 조건을 따라야 합니다:



저작자표시. 귀하는 원저작자를 표시하여야 합니다.



비영리. 귀하는 이 저작물을 영리 목적으로 이용할 수 없습니다.



변경금지. 귀하는 이 저작물을 개작, 변형 또는 가공할 수 없습니다.

- 귀하는, 이 저작물의 재이용이나 배포의 경우, 이 저작물에 적용된 이용허락조건을 명확하게 나타내어야 합니다.
- 저작권자로부터 별도의 허가를 받으면 이러한 조건들은 적용되지 않습니다.

저작권법에 따른 이용자의 권리는 위의 내용에 의하여 영향을 받지 않습니다.

이것은 [이용허락규약\(Legal Code\)](#)을 이해하기 쉽게 요약한 것입니다.

[Disclaimer](#)

공학석사학위논문

위치 특이적으로 고안된 실리콘 나노리본
기반의 장치를 이용한 다기능성 전자 피부

**Multifunctional electronic skin using site-specifically
designed silicon nanoribbon devices**

2015년 7월

서울대학교 대학원

협동과정 바이오엔지니어링

이 민 철

**Multifunctional electronic skin using site-
specifically designed silicon nanoribbon
devices**

**A THESIS SUBMITTED IN PARTIAL FULFILLMENT OF THE
REQUESTMENTS FOR THE DEGREE OF MASTER IN ENGINEERING
AT THE GRADUATE SCHOOL OF SEOUL NATIONAL UNIVERSITY**

July 2015

By

Mincheol Lee

Supervisor

Day-Hyeong Kim

Abstract

Multifunctional electronic skin using site-specifically designed silicon nanoribbon devices

Mincheol Lee

Interdisciplinary Program for Bioengineering

The Graduate School

Seoul National University

Advances in prosthetic technology facilitate amputees' restoring movements to the missing body parts. An accurate restoring motor function of missing parts requires feedback of sensory signals from the prosthesis as actual human skin. However, despite the advances, providing sensory function to prosthesis and connecting the sensory function to the nerve system are still challenging. To provide prosthesis with sensing abilities, researches on electronic skin with various sensors and materials were conducted. But with limited performances such as stretchability, detection range, and spatio-temporal resolution, it was difficult to mimic actual human skin. Here, a stretchable, electronic skin

with various sensing capabilities: strain, pressure, and humidity is demonstrated. Using site-specifically designed monocrystalline silicon nanoribbon, high sensitivity and enhanced range of sensing ability under the skin deformation are achieved. For connecting the signals from electronic skin to the nervous system, transmission of sensed signals to the nervous system is performed, from the peripheral nerve to the brain, using stretchable multi-electrode arrays decorated with neuro-protective nanoparticles. Combined with sensory and actuating functions, this system provides an effective solution for emerging classes of prostheses.

Keywords: Stretchable electronics, flexible electronics, electronic skin, physiological signal monitoring.

Student number: 2013-23195

Contents

1. Introduction.....	1
2. Site-specifically designed silicon nanoribbon based sensors.....	3
2.1 Heterogeneous nature of skin-deformation depends on location.....	3
2.2 Material characterization of single crystalline silicon for strain sensor	8
2.3 SiNR strain gauges with different curvatures.....	10
2.4 SiNR pressure sensors with serpentine design.....	15
3. Metal based humidity sensor and heater with stretchable designs	19
3.1 Characterization of humidity sensor	19
3.2 Characterization of stretchable heater	24
4. Sensing capability of electronic skin in simulated daily life	27
5. Connecting electronic skin and nervous system	33
5.1 Low impedance multi-electrode array with neuro-protective nanoparticles.....	34
5.2 Stretchable multi-electrode array contacting peripheral nerves	37
5.3 In vivo experiment of interfacing electronic skin with nervous system	39
6. Experimental Section.....	41
7. Conclusion.....	47
8. References.....	48

List of Schemes

1. Setup of motion-capturing system	5
2. Setups for characterization of humidity sensor	20
3. Capacitive type humidity sensor and schematic diagram of humidity sensing mechanism	21
4. Overall scheme of interconnection between electronic skin to nervous system	35

List of Figures

1. Regional strain distribution of skin segments of hand for various motions.....	6
2. Map of maximal stretching range for whole area and designed SiNR strain sensors correspondingly to the ranges	7
3. Transmission electron microscopy images of doped single crystalline silicon	9
4. Images of SiNR strain gauges with different curvatures under different strains and FEA results	12
5. Resistance changes of SiNR strain gauges with different curvatures depend on applied strain and cyclic stretching tests	13
6. Spatial maps of percent resistance changes measured by site-specifically designed strain gauges for various motions	14
7. Schematic image of the working principle of the pressure sensor	16
8. Illustration of stretching test with pressure sensor and relative resistance changes of pressure sensor with stretching test as function of applied pressure.....	17
9. Experimental set-up for stretching test with pressure sensor array and Spatial maps of percent resistance changes measured by pressure sensor array	18
10. Calibration curves and temporal sensitivity of humidity sensors	22
11. Image of water droplets covering humidity sensor array and regional capacitance change.....	23
12. Heating capability of stretchable heater	25
13. Stability of heater under applied strains	26

14. Characterization of SiNR strain sensor on prosthetic hand performing handshakes	29
15. Characterization of SiNR pressure sensor on prosthetic hand performing keyboard tapping	30
16. Characterization of humidity sensor on prosthetic hand touching dry and wet diapers, and corresponding capacitance changes of humidity sensor	31
17. Characterization of heater conducting heat transfer from prosthetic hand to baby doll	32
18. Scanning electron microscopic image of PtNWs. Frequency response of impedance of PtNW/Au electrodes. Effect of ceria nanoparticles on ROS scavenging performance	36
19. Fabricated stretchable MEA and FEA results of MEA with and with out serpentine mesh structure. Administration of stretchable MEA by wrapping sciatic nerves of rat	38
20. (a) Schematic diagram of experiment for stimulation with signal from the pressure sensor on electronic skin. (b) Measured signals from pressure sensor on electronic skin, applied voltage on sciatic nerve according to the pressure signal and injected current signal through the nerve, acquired EEG signal from the VPL of thalamus in the right hemisphere	40

1. Introduction

Skin with sensory receptors plays an important role in obtaining information from the external environment.¹ Especially, our ability to manipulate objects freely with hands relies on cutaneous sensation of external stimulation such as pressure, heat, and pain.² The afferent nervous system delivers the cutaneous sensory inputs to the central nervous system and the information is analyzed and transformed into regulated physiological signals for motor control.¹ In researches on prosthetic engineering, there have been efforts to make prosthesis mimicking the physiological mechanism of sensation.²⁻⁵ Although there have been progresses in replicating the cutaneous sensation using prosthetic limbs integrated with tactile sensors in rigid or semi-flexible forms, there still remain issues in sensing performances and mechanical properties of established sensors in prosthetic devices which are different from soft skin tissues.

In order to overcome those limitations of established artificial sensory system on prosthesis, flexible and/or stretchable tactile sensors using micro/nano materials and structures have been studied.⁶⁻¹¹ Particularly, pressure-sensitive rubber (PSR) based resistive type tactile sensors¹²⁻¹⁴, which can be integrated with organic material¹⁵⁻¹⁸ and nanomaterial^{19,20} based transistors, have been studied with an intense focus. However, conventional PSR based sensors are susceptible to hysteresis and have limitation in response time. As an alternative to PSR, single crystalline silicon, which exhibits a linear relationship between resistance change and strain with fast response time, are used for

mechanical sensor. Combined with soft elastomeric substrate, single crystalline silicon based mechanical sensor have been used to detect motions at various body parts, such as the wrist²¹ and fingers²². Besides, with stretchable design, single crystalline silicon and metal based temperature sensors²³ fabricated on ultrathin polymeric substrate have been utilized for temperature monitoring on human skin²³. Those sensors, however, cannot reflect the heterogeneity in geometry and strain profile of skin at different site on the body. Therefore, custom-designs for specific body locations reflecting site-specifically varied degree of skin-deformation according to movements of the body are necessary.

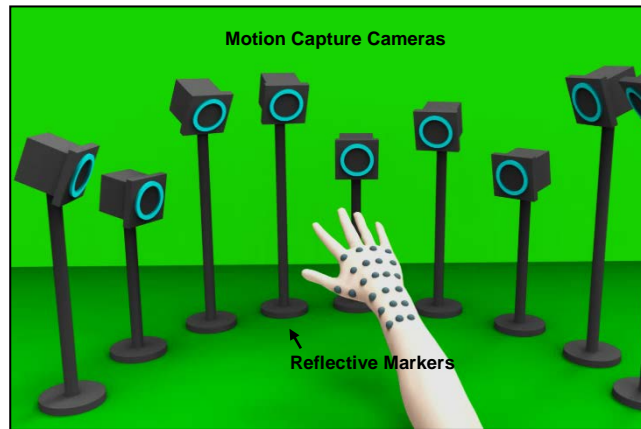
In this paper, a stretchable electronic skin equipped with single crystalline silicon nanoribbons (SiNRs) strain sensor for movement sensing. Because the SiNR sensor arrays are designed to stretch in accordance with the dynamic mechanical properties of the target skin segment, the electronic skin provides enhanced spatio-temporal sensitivity and mechanical reliability. Besides, metal-based, humidity sensor and heater are integrated with electronic skin to facilitate the sensation of moisture around skin and body temperature regulation, individually. Perception capabilities of proposed electronic skin are proved in diverse simulated situation related daily life. And this work also shows that electrical signals acquired from sensors on electronic skin can be transmitted through the afferent nervous system via conformally contacted stretchable electrode decorated with neuro-protective ceria nanoparticles, which mimics physiological sensation mechanism in body.

2. Site-specifically designed silicon nanoribbon (SiNR) based sensors

2.1 Heterogeneous nature of skin-deformation depends on location

Because skin-segments at different locations experience multi-axial forces and differently deform following linear and angular movements, it is essential to know the actual distribution of skin stretching range in specific motion for developing the artificial skin whose tactile sensing functionalities are optimized for it. To measure the regional skin stretching range, motion capture system (Scheme 1) is used for temporal movement monitoring of several particular points of the target region on skin in specific motion. Twelve high-end motion capture cameras (OptiTrack Prime 41, NaturalPoint, USA) acquired the relative three-dimensional coordinates of reflective markers attached on the subject's hand in real time. Considering multi-axial forces on the skin at the hand, four different representative hand motions, clenching fist, front bending, tilting towards left and right, are analyzed to map regional strain distinctly varied with the motion of the hand (Fig. 1). The mapped images are obtained by interpolating the strain calculated by measured displacement of adjacent reflective markers (Experimental Section 6.2) relative to the initial locations of them. In case of clenching the fist, the skin is hardly stretched only up to 5% (Fig. 1, upper left). However, relatively large strain up to 16% is applied in wide range on the wrist in case of front bending of the hand (Fig. 1, upper right). In

addition, tilting hand induces compression on the tilting direction side of the wrist skin (Fig. 1, bottom left) while the other side is stretched (Fig. 1, upper left). By gathering up these data, the map of maximum strain on the hand skin can be extracted as shown in the Fig. 2. Serpentine designs, which can accommodate strains, are applied on stretchy areas, to accommodate the larger range of strain changes. For regions where skin hardly stretches, linear type is designed to maximize sensitivity due to its relatively low resistance.



Scheme 1. Setup of motion-capturing system.

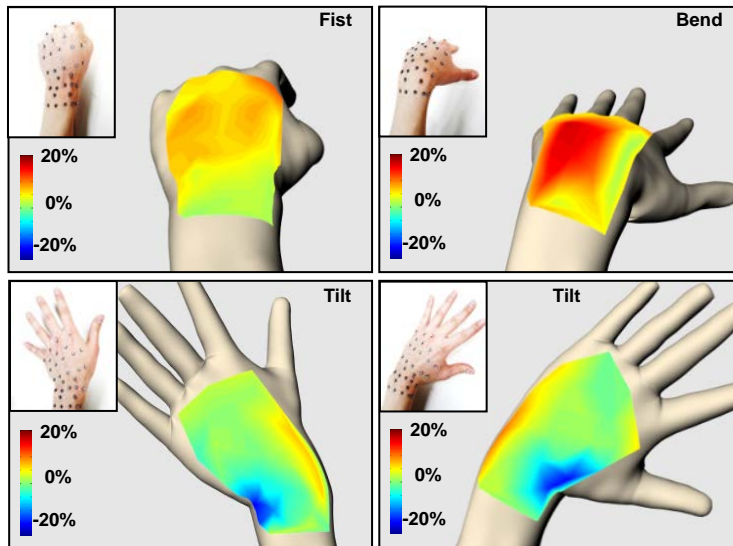


Figure 1. Regional strain distribution of skin segments of hand for various motions.

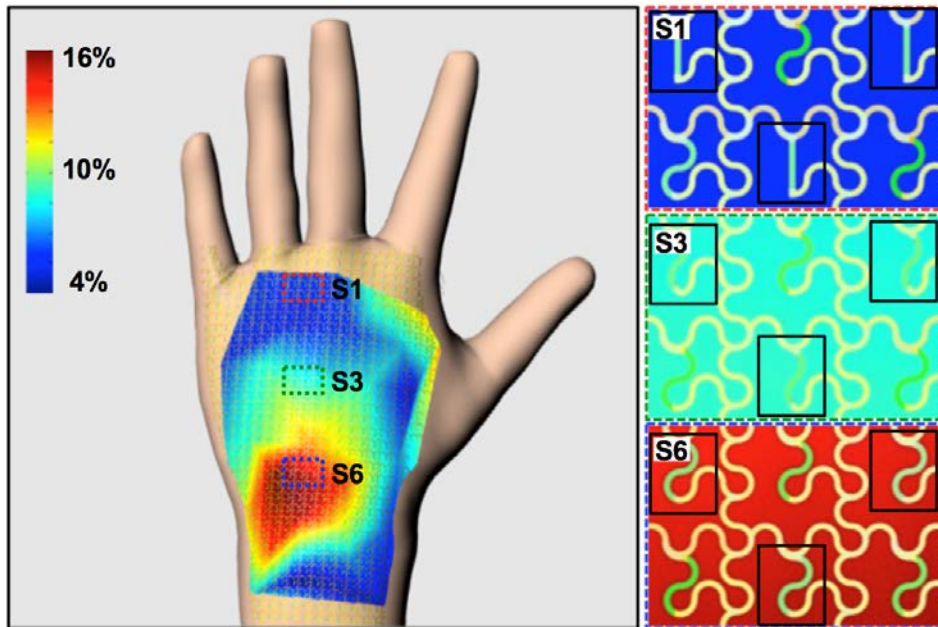


Figure 2. Map of maximal stretching range for whole area and designed SiNR strain sensors correspondingly to the ranges.

2.2 Material characterization of single crystalline silicon for strain sensor

Strain sensor for delicate movement monitoring, which is important for controlling prosthetic device, is one of the most necessary components. For effective sensing, sensor of resistance type with minimum hysteresis and relatively fast response time is beneficial. To satisfy the conditions, strain sensors are fabricated p-type doped single crystalline SiNRs, which have both high piezoresistivity (gauge factor: ~ 200)²¹ and low fracture toughness ($\sim 1.0 \text{ MPa m}^{1/2}$)²⁴. p-type doped single crystalline SiNRs are fabricated with silicon on insulator (SOI, Si(140nm)/SiO₂/Si) wafer by spin on dopant process. Detailed fabrication process of SiNR is represented in experimental section 6.1. Figure 3 show Transmission electron microscopic (TEM) image of doped SiNR transfer printed on polyimide (PI) substrate. The thickness of silicon layer is slightly decreased but electron energy loss spectroscopic image (red dotted box) of doped region shows that boron-doped region is geometrically well confined. To minimize stresses on active layer of silicon while bending or stretching, neutral plane configuration²⁵ with ultrathin ($\sim 110\text{nm}$) SiNR is used.

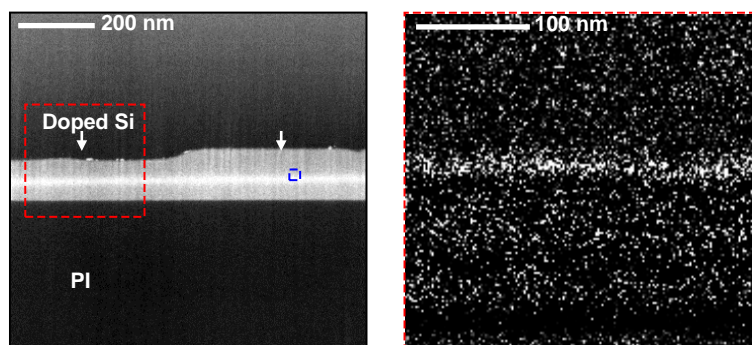


Figure 3. Transmission electron microscopy (TEM) images of doped single crystalline silicon (left). Red dotted box (right) indicates electron energy loss spectroscopy map of boron (white dots).

2.3 SiNR strain gauges with different curvatures

Suitability of the site-specifically designed SiNR based on different ranges of strain, stretching tests with SiNR strain gauges comprised of six serpentine designs having different curvature: $\kappa = 0$ (S1), 1.94 (S2), 4.74 (S3), 7.4 (S4), 9.75 (S5), 10 mm^{-1} (S6) are conducted. Figure 4 shows the SiNR strain gauge array under stretching test (from 0% to 30%) and corresponding finite element analysis (FEA) results. As applied strain increases, the SiNR strain gauges with small curvature experience considerable amount of strain compared to the designs with larger curvature because the serpentine shape of larger curvature can better relieve accumulation of strain by changing its shape.

The ratio of relative change in resistance to initial one ($\Delta R/R$) for each SiNR design as a function of applied strain shows the results in accordance with the FEA results: the SiNR of larger curvature endures more applied strain and shows lower sensitivity (Fig. 5, left). The SiNR S6 was able to sustain strain-sensing capability up to 30% of applied strain whereas S1 was broken at lower than 10% of applied strain. Conversely, cyclic stretching test results reveal that the sensitivity of the devices increases with the decrement in curvature of SiNR (Fig. 5, right). The results also exhibits that the SiNR strain gauge shows highly linear and fast response regardless of the design. With its compliant characteristic with applied strain, the serpentine shape of SiNR counteracts the stress applied to it, and this reduces the device sensitivity at larger curvature design. According to this balancing effect, SiNR S1, which has the highest sensitivity, is appropriate for the sites with small range of stretching to measure the applied strain

precisely, whereas S6 is suitable for the locations with wide range of stretching due to its high stretchability.

Site-specifically designed strain gauge arrays conformally attached on the hand are used to prove its regional strain sensing capability. Figure 3c shows the strain maps on the back of hand and wrist in four representative motions using site-specific SiNR strain gauges, measured using signal measurement unit with multiplexing units (experimental section 6.4). To map minimally applied regional strain on the back of hand in motion of closing fist, SiNR strain gauge array of S1 is used (Fig. 6, upper left). Despite of the small amount of applied strain on the back of hand (Fig. 1, upper left), the SiNR strain gauge array of S1 can measure the regional strain with high sensitivity. Conversely, SiNR strain gauge array of S6 is used to map regional strain of wide range on the wrist in motion of bending (Fig. 6, upper right) and tilting (Fig. 6, bottom left and right). Despite of the relatively large applied strain on the wrist (Fig. 1, upper right, bottom left and right), the SiNR strain gauge array of S6 can measure the regional strain with mechanical stability.

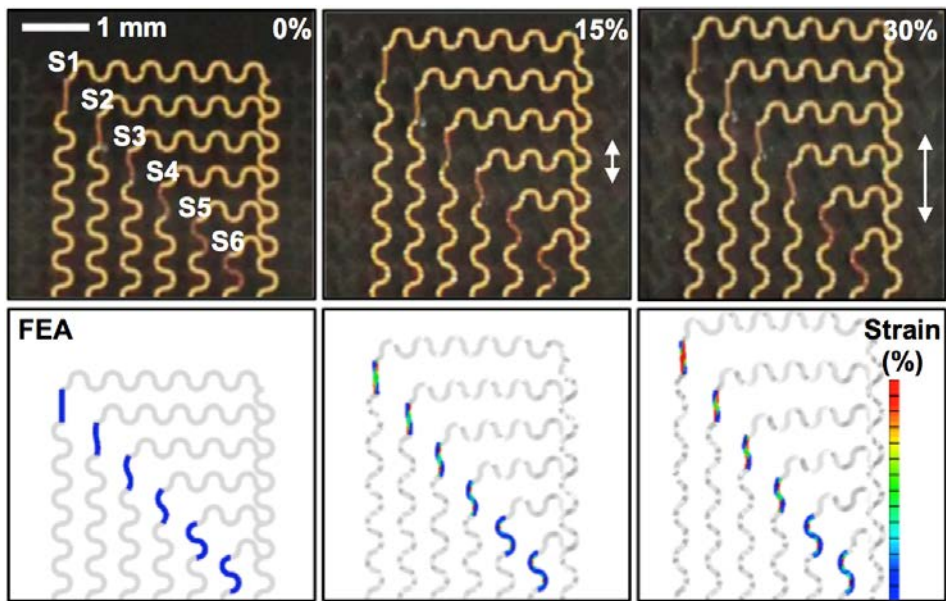


Figure 4. Images of SiNR strain gauges (top row) with different curvatures under different strains (0%, 15%, 30%) and FEA results (bottom row).

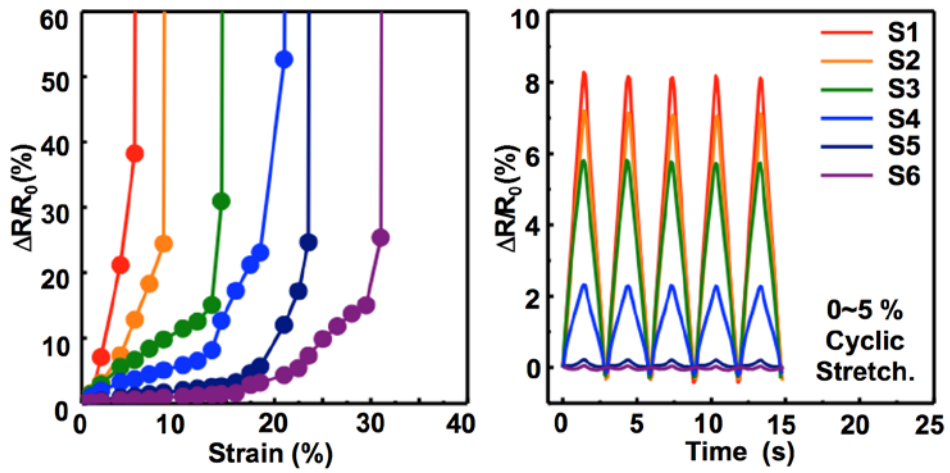


Figure 5. Resistance changes of SiNR strain gauges with different curvatures depend on applied strain (left) and cyclic stretching tests (right).

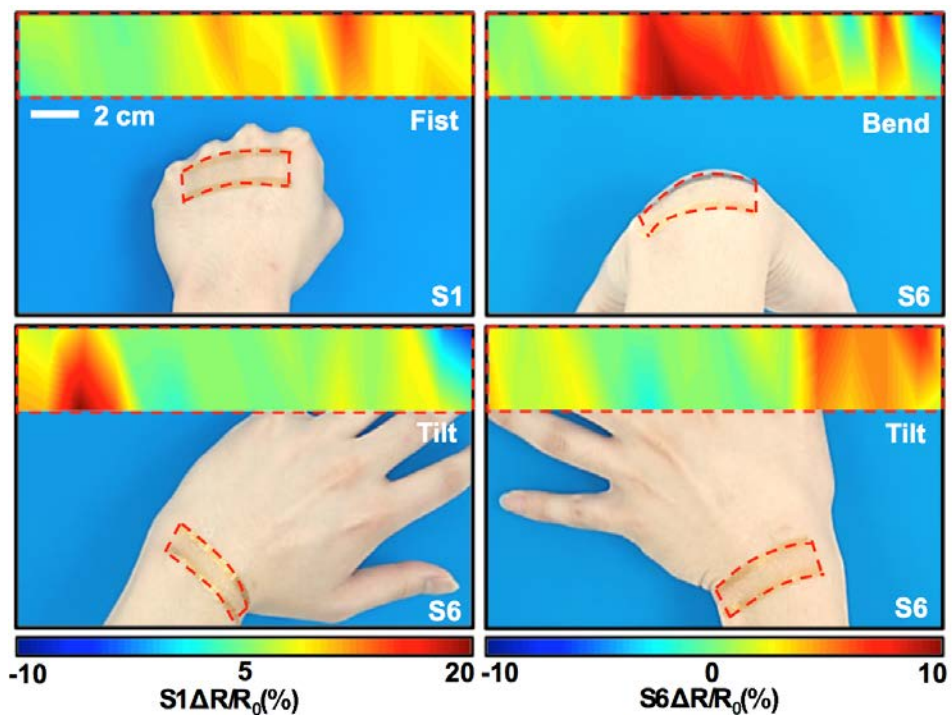


Figure 6. Spatial maps of percent resistance changes measured by site-specifically designed strain gauges for various motions.

2.4 SiNR pressure sensors with serpentine design

Figure 7 shows the scheme of the pressure sensor, which is one of the key components for the tactile sensing. By introducing a cavity into the PI passivation layer of the SiNR strain gauge, the pressure-induced strain applied to the SiNR is expected to enlarge as compared to the strain gauge of no cavity in the PI passivation layer because sensing point of pressure is off the neutral plane. Applying controlled pressure on the SiNR tactile sensor revealed that the one with a cavity presented about ten times higher pressure sensitivity than the one with no cavity (fig. 7, strain sensor): measured sensitivity of of S6 were 0.075/kPa (with cavity), 0.0073/kPa (without cavity) respectively. S6 type of design is used for pressure sensor to minimize effect of strain on pressure sensor. As illustrated in Figure 8, with serpentine S6, pressure sensor sensing capability does not change much according to stretching (10%). S1 design is also can be used for hardly stretchy region of skin. Similar to strain sensors with various curvatures of serpentine, pressure sensor with S1 design has higher (almost 4 times) sensitivity than sensor with serpentine of S6 design. With array configuration, mapping test of applied pressure is conducted and figure 9 shows regionally mapped pressure.

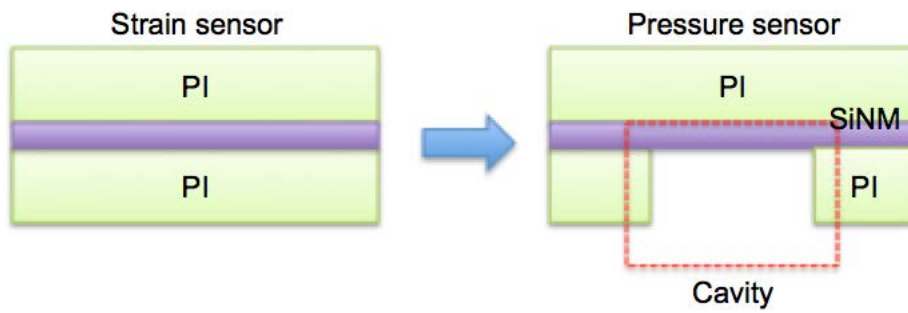


Figure 7. Schematic image of the working principle of the pressure sensor.

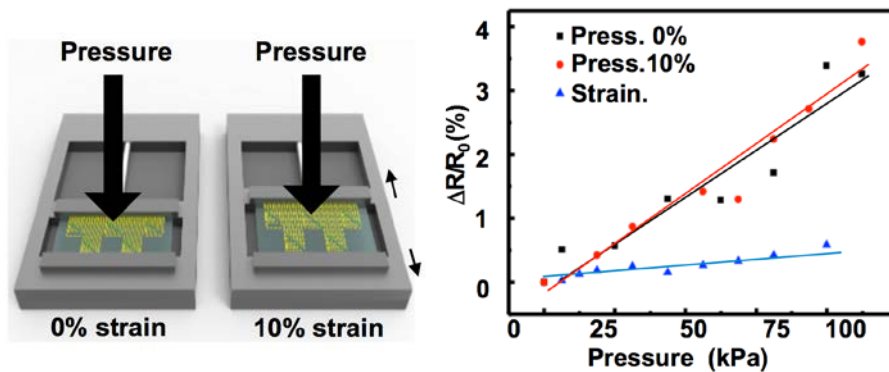


Figure 8. Illustration of stretching test with pressure sensor (left) and relative resistance changes of pressure sensor with stretching test as function of applied pressure (right). Strain sensor (no cavity) is also tested with applied pressure (blue triangle). Press., pressure sensor.

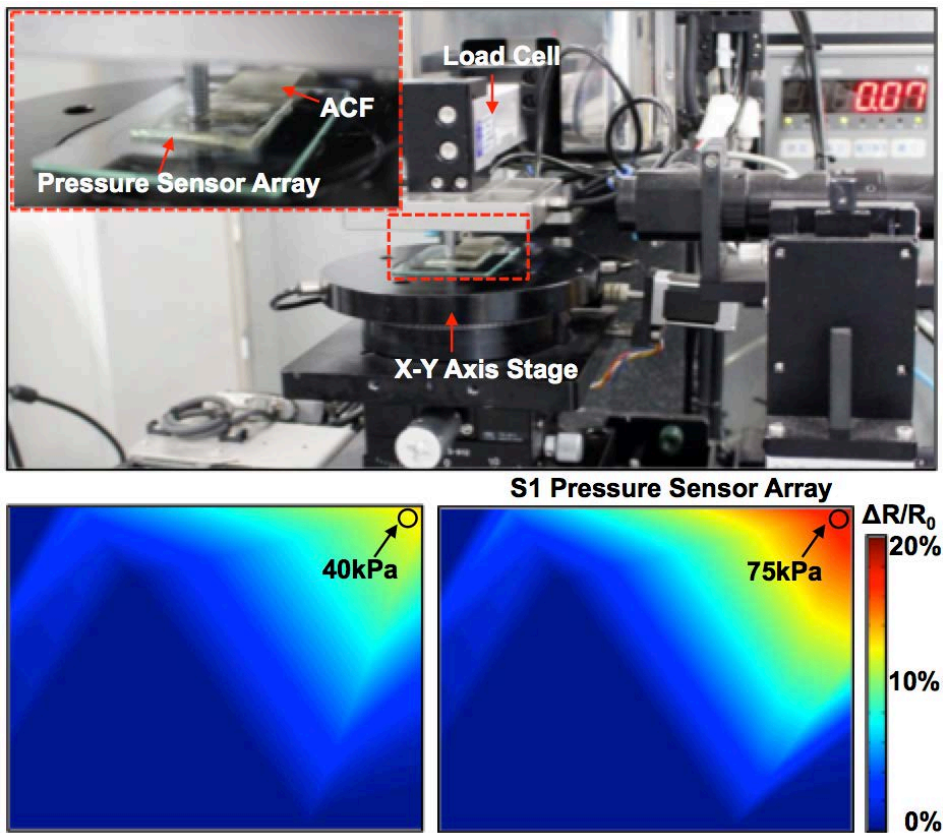
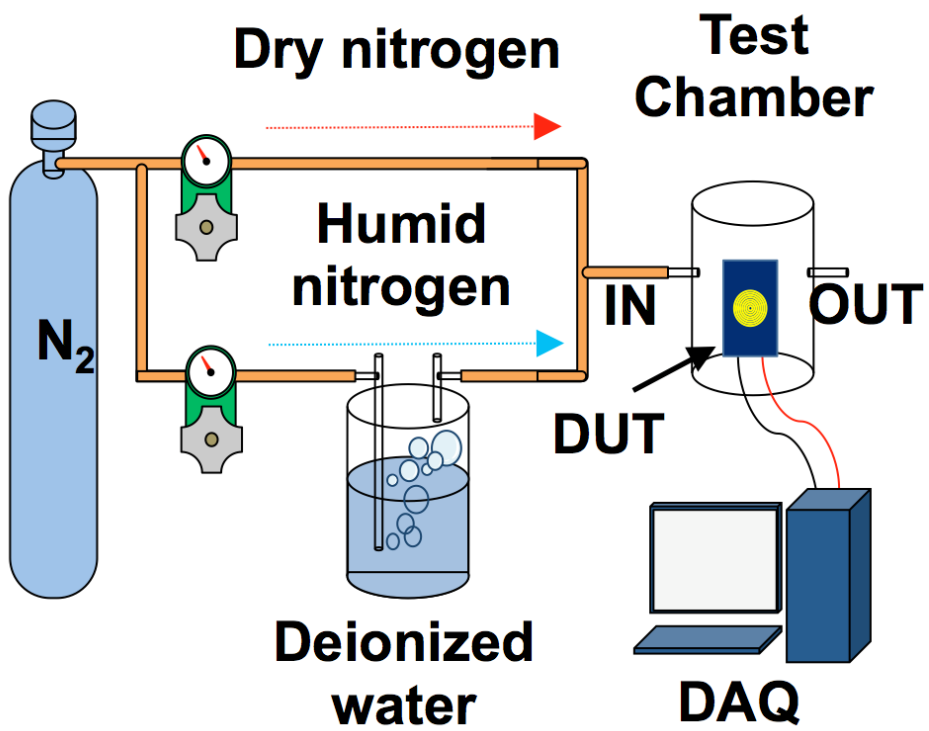


Figure 9. Experimental set-up for stretching test with pressure sensor array (top) and regional map of percent changes of resistances to applied pressure (40kPa, 75kPa) (bottom).

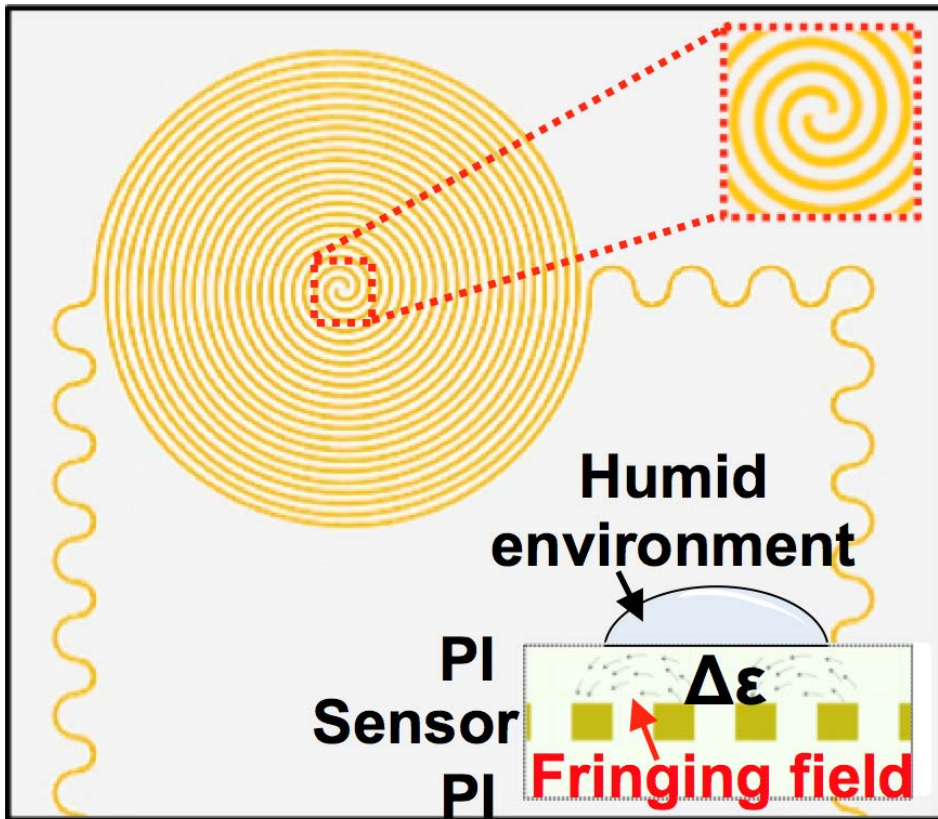
3. Metal based humidity sensor and heater with stretchable designs

3.1 Characterization of humidity sensor

There are no specific receptors for humidity in the human skin. However, the human skin can sense the humidity around atmosphere by combining the sensations of mechanoreceptors and thermoreceptors²⁶. In artificial skin, I fabricated a capacitive humidity sensor array for the artificial skin to provide the sensation of humidity. The humidity sensing was performed in the test chamber where the humidity was freely controllable (Scheme 2). The proposed humidity sensor array senses the capacitance change induced by permittivity change of the PI which absorbs water well (Scheme 3). A calibration curve (Fig. 10, left), shows fabricated humidity sensor react properly to the change of relative humidity. Besides, overlapped traces of the relative humidity measured by the commercial humidity sensor and the relative capacitance change measured by the fabricated humidity sensor prove the humidity sensing capability of the proposed humidity sensor (Fig. 10, right). The regional humidity sensing is available when the humidity sensor is fabricated in array (Fig. 11). So the artificial skin equipped by the proposed humidity sensor array can sense the humidity distribution mimicking the actual skin.



Scheme 2. Setups for characterization of humidity sensor.



Scheme 3. Capacitive type humidity sensor and schematic diagram of humidity sensing mechanism.

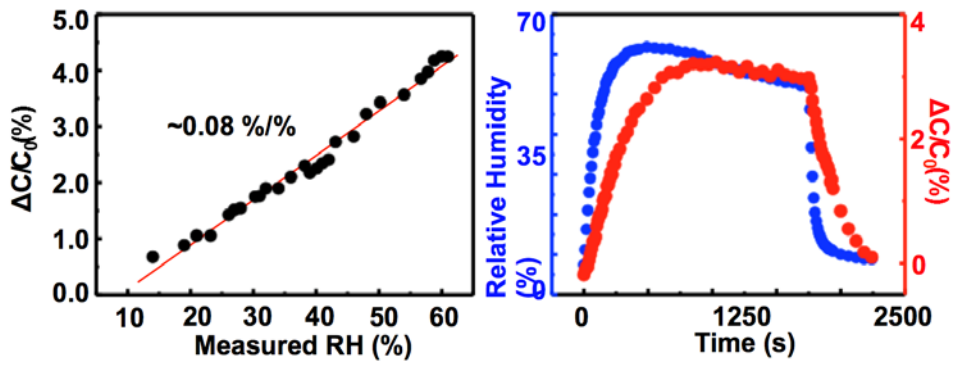


Figure 10. Calibration curve of humidity sensor (left) and temporal sensitivity of humidity sensor (red) compared to commercial sensor (blue).

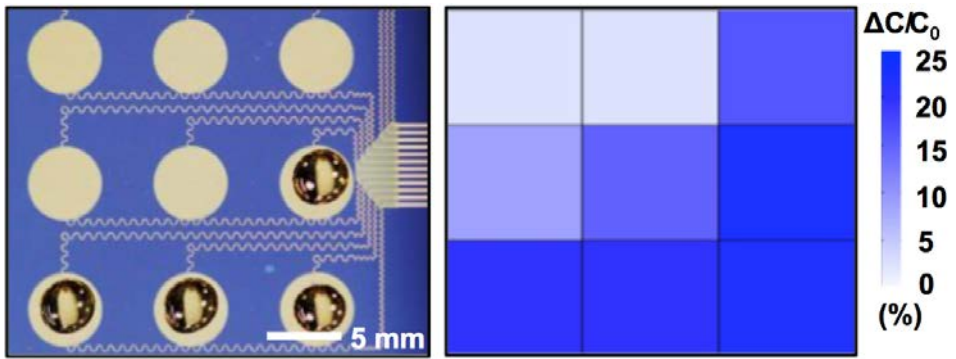


Figure 11. Image of water droplets covering humidity sensor array and regional capacitance change.

3.2 Characterization of heater

The users of prosthetic limbs communicate with another person or animals by touching in their daily life. To ease incompatibility, prosthetic limbs can touch them as close as the real one, not only its mechanical properties, but also its temperature. In this regard, temperature of prosthetic skin should be similar as possible compared to that of the human body. To satisfy the condition, a stretchable heater with fractal-like design²⁷ is incorporated in electronic skin. This actuator can maintain the body temperature (Fig. 12, left). And it can represent even higher temperature (Fig. 12, right) for additional practical purposes such as warming or drying. This thermal actuating performance is maintained with negligible change in case of from slight stretching (Fig. 13, left, ~5%) to extreme stretching (Fig. 13, right, ~20%).

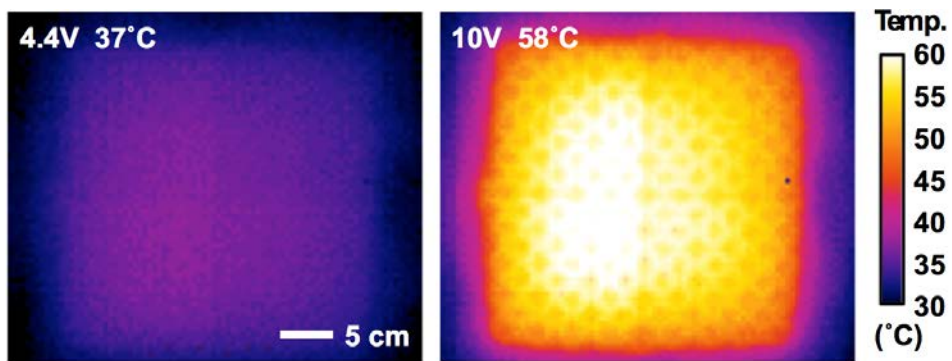


Figure 12. Heating capability of stretchable heater; emulating human body temperature (left) and higher temperature (right).

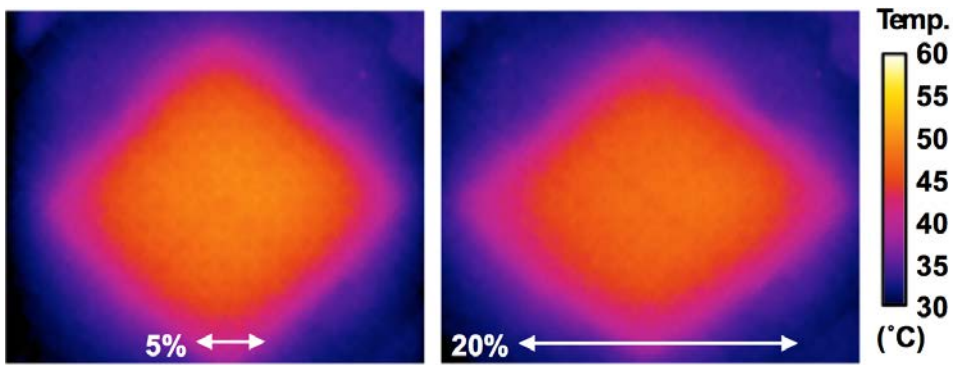


Figure 13. Stability of heater under applied strains (5%: left, 20%: right).

4. Sensing capability of electronic skin in simulated daily life

The prosthetic hand covered by the proposed electronic skin is simulated with several daily situations such as hand shaking, keyboard tapping, touching dry/wet diaper, and cuddling baby. In case of the shaking hand using the prosthesis, the spatiotemporal strain information is successfully monitored by SiNR strain gauge array of S1 (Fig 14). Despite of minimal applied strain, the map of the applied strain is obtained by high sensitivity of strain sensor with S1 design, showing that the skin area of knuckle around index finger is more stretched than that of little finger when the prosthetic hand grabs a human hand (Fig. 14). For investigating the performances of SiNR pressure sensor (S6) of the artificial skin, the temporal resistance change is observed while the prosthetic hand is tapping the keyboard (Fig. 15). The pressure sensor shows reliable performance for relatively rapid stimuli. When people caring baby decide whether they should replace the diaper or not, they usually touch the surface of it and try to sense the humidity. Similarly, the prosthetic hand equipped by the artificial skin with humidity sensing capability touched both dry (Fig. 16, left top) and wet diaper (Fig. 16, left bottom). The measured capacitance differences between dry and wet cases are clearly distinguished. In case of touching wet diaper, the capacitance is increased for 2.77% while 0.31% of capacitance decreases in case of dry diaper (Fig. 16, right). As mentioned above, it is important to make the prosthetic hand as warm as the actual hand for preventing the baby feels incompatibility

while the amputees are touching their baby (Fig. 17, left). The proposed artificial skin with stretchable heater was heated up to the 36.5°C (Fig. 17, middle) and the transfer of this warmth to the different spot of the baby is demonstrated (Fig. 17, right).

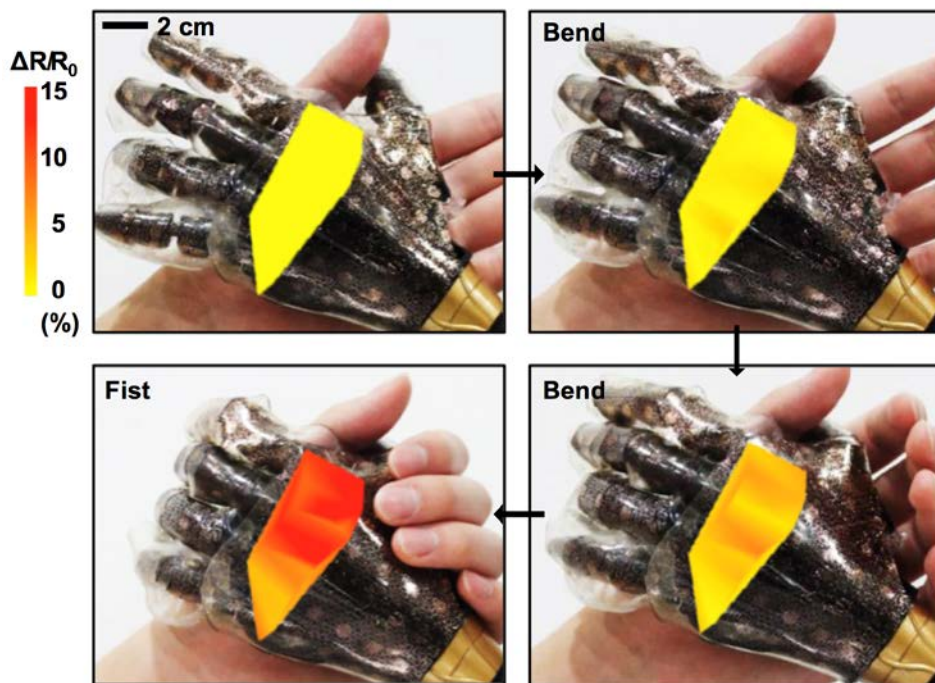


Figure 14. Characterization of SiNR strain sensor on prosthetic hand performing handshakes.

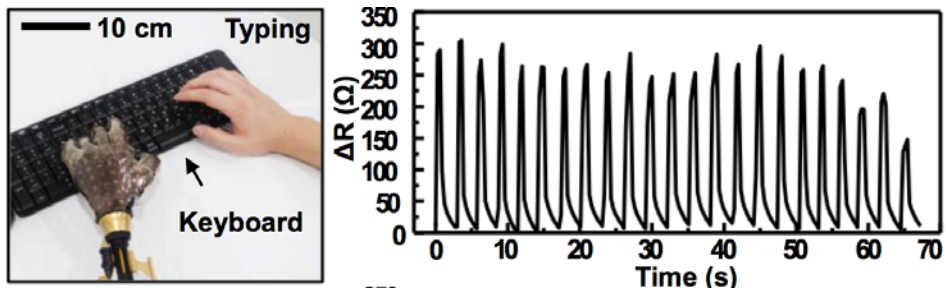


Figure 15. Characterization of SiNR pressure sensor on prosthetic hand performing keyboard tapping.

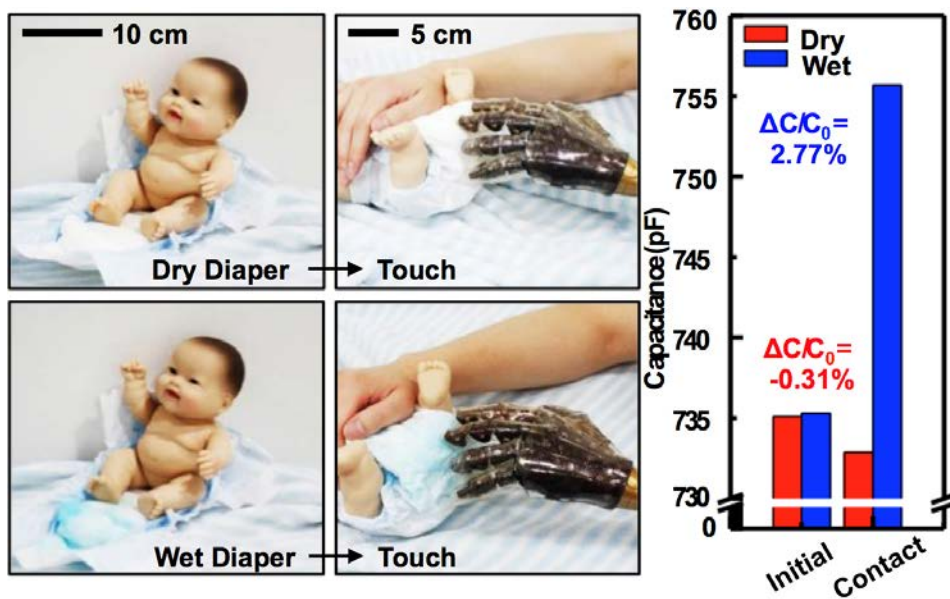


Figure 16. Characterization of humidity sensor on prosthetic hand touching dry (left top) and wet (left bottom) diapers and corresponding data of capacitance change of humidity sensor.

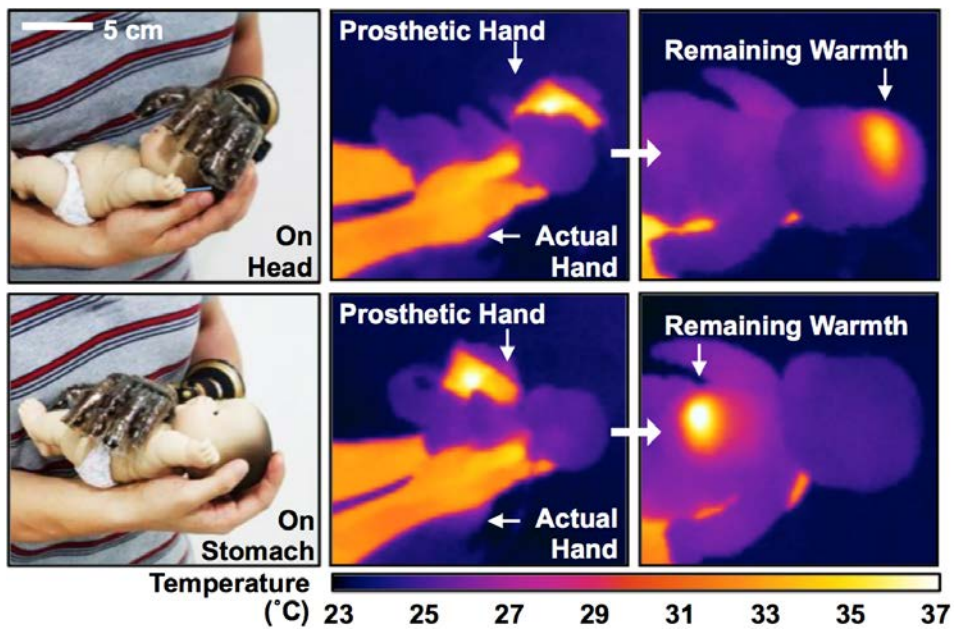


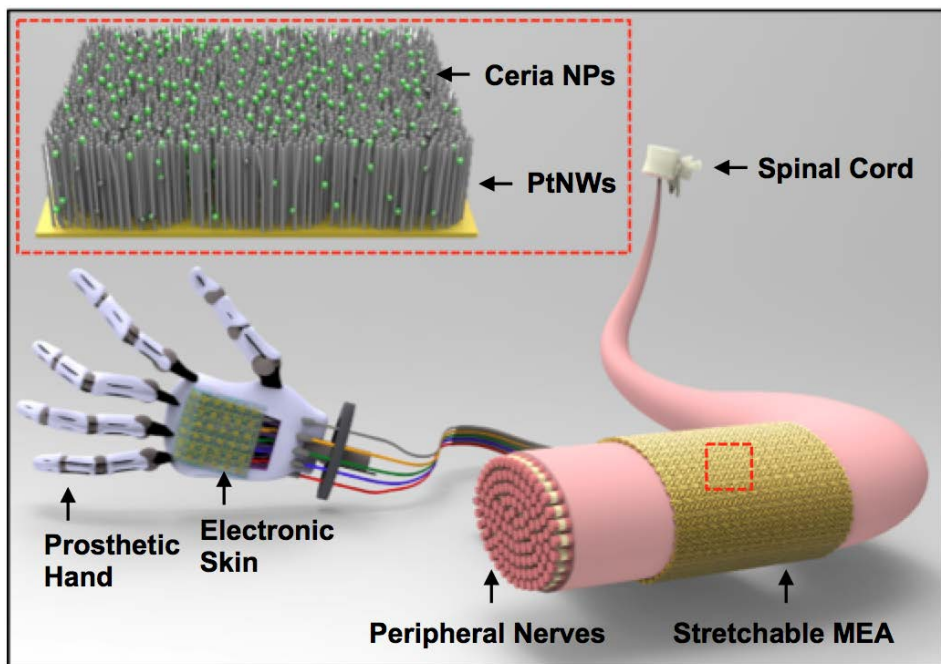
Figure 17. Characterization of heater conducting heat transfer from prosthetic hand to baby doll.

5. Connecting the electronic skin and nervous system

The ultimate goal of skin prosthesis is to enable amputees to feel various types of external stimuli. To achieve this goal, the signals captured across various sensor arrays must be processed and transmitted to stimulate the corresponding peripheral nervous system (Scheme 4). For effective charge injection to peripheral nerves, low impedance in MEA²⁸ is critical. In addition, there are various mechanical motions of adjacent muscles, which require deformations of the interfacing electrodes to preserve mechanical contact. Furthermore, inflammations at interfaces between electrodes and nerves by mechanical mismatches²⁹ must be suppressed.

5.1 Low impedance multi-electrode array with neuro-protective nanoparticles

The MEAs are decorated with platinum nanowires (PtNWs, Fig. 18 left) for low impedance for sensing quality. PtNWs are grown using an electrochemical method with anodic aluminum oxide (AAO) nanostructures as templates. Ceria nanoparticles are coated on PtNWs to suppress the reactive oxygen species (ROS) generation that is neurotoxic at high concentration³⁰. The low impedance characteristic of Pt and increase of active interfacing area between electrode and neural surface by NWs decrease impedance significantly lower than that of planar only Au or Pt electrodes (Fig. 18 middle). Ceria nanoparticles decorated on PtNWs successfully scavenge ROS (Fig. 18 right), which prevents ROS-induced inflammations³¹.



Scheme 4. Overall scheme of interconnection between electronic skin to nervous system.

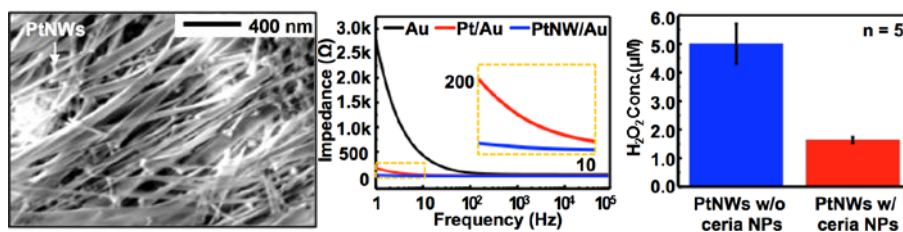


Figure 18. Scanning electron microscopic image of PtNWs (left). Frequency response of impedance of Au (black), Pt/Au (red) and PtNW/Au (blue) electrodes (middle). Effect of ceria nanoparticles on ROS scavenging performance (right, blue: PtNWs without ceria nanoparticles; red: PtNWs with ceria nanoparticles).

5.2 Stretchable multi-electrode array contacting peripheral nerves

Figure 19 shows the fabricated stretchable MEA (left) and FEA result (middle) shows that much lower shear stress is applied to the nerve fiber with the stretchable, serpentine-mesh type MEA than the flexible, planar-sheet type MEA. For experimental verification, in a Sprague Dawley rat, the sciatic nerve is exposed after the gluteus muscles are dissected (Experimental section 6.5). The stretchable MEA is wrapped around the nerve fiber (Fig. 19 right) and maintains conformal contacts under deformations (Fig. 19 right inset). Wrapping the nerve fiber with the stretchable MEA is conducted by removing sacrificial layer (polyvinyl alcohol, PVA) under the MEA. Additional mechanical-stress-induced inflammations³² can be prevented by virtue of the ceria nanoparticles adsorbed on the stretchable MEA.

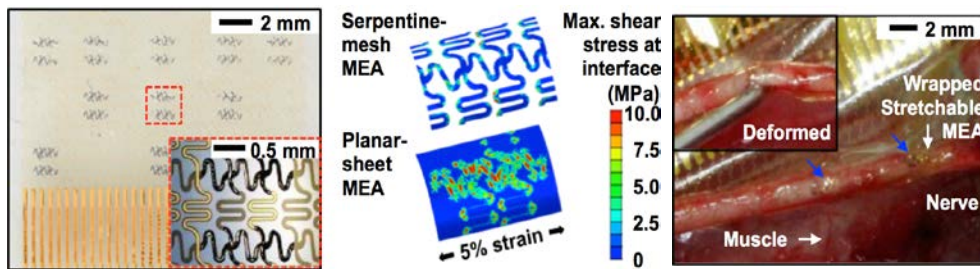


Figure 19. Fabricated stretchable MEA (left) and FEA results of MEA with and with out serpentine mesh structure (middle). Administration of stretchable MEA by wrapping (right) sciatic nerves of rat.

5.3 In vivo experiment of interfacing electronic skin with nervous system

In vivo electrophysiological recording from the ventral posterolateral nucleus (VPL) is performed^{33,34}. Recording electrodes are positioned in the VPL of the thalamus (Anteroposterior: -2.3 mm, Medio-Lateral: 3.0 mm, Dorso-Ventral: -6.0 to -7.0 mm) in the right hemisphere (Fig. 20a). Signals from the fabricated pressure sensor (black, Fig. 20b top) are obtained and processed as input signals (red) injected through stretchable MEA (Fig. 20b middle). Flowing current (blue) by applied voltages (red) through nerves are measured (Fig. 20b middle). Evoked potentials of the rat's VPL are simultaneously measured (Fig. 20b bottom, experimental section 6.6). Recorded electrophysiological signals synchronized input signals from the pressure sensor. And this indicates electrical signal injection is successfully conducted into the peripheral nerves and transferred to central nervous system. Although in this paper noticeable advances using the nanomaterials-decorated stretchable neural interfaces are represented, safety issues can be brought up, such as fractured PtNWs in bloodstream and long-term stability of electrodes and dose of ceria nanoparticles, which should be clarified in the future study.

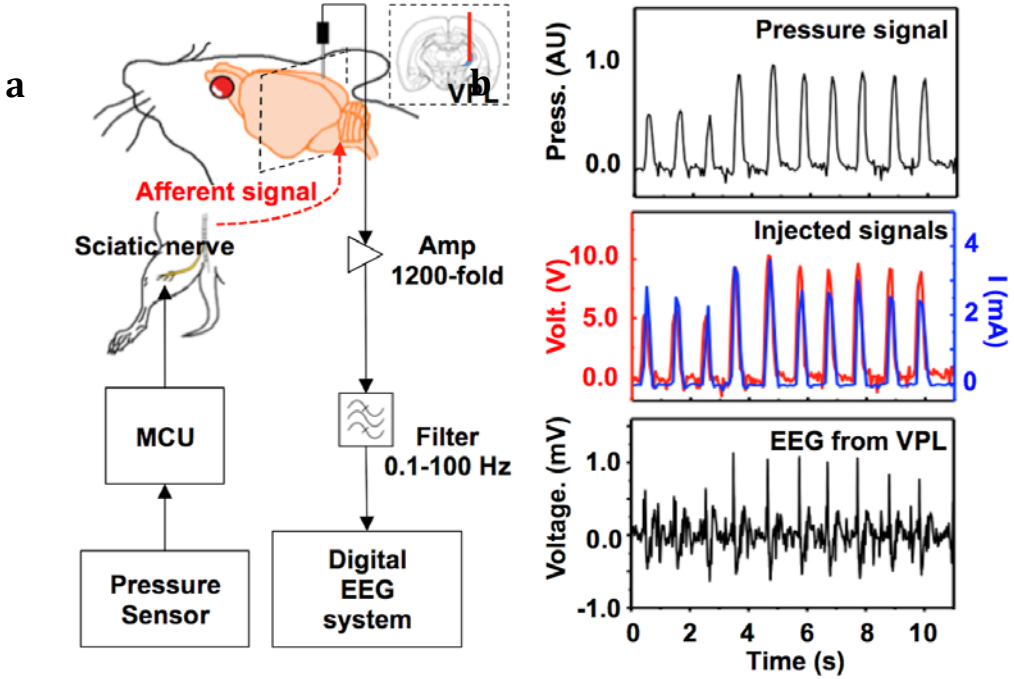


Figure 20. (a) Schematic diagram of experiment for peripheral stimulation with signal from the pressure sensor on electronic skin. (b) Measured signals from pressure sensor on electronic skin (top), applied voltage (red, middle) on sciatic nerve according to the pressure signal and injected current signal (blue, middle) through the nerve, acquired Electroencephalography signal from the VPL of thalamus in the right hemisphere (bottom).

6. Experimental section

6.1 Fabrication SiNR-based devices

The fabrication begins with doping of silicon-on-insulator wafer with spin-on-dopant. The doped regions are transfer printed onto PI film coated on a silicon oxide (SiO₂) wafer.

Using reactive

ion etching with ph

Thermal evaporation for metallization (Au/Cr, 70 nm/7 nm), photolithography and wet-etching steps define the serpentine metal lines. Top PI layer is spin coated and the entire trilayer (PI/device/PI) is patterned by reactive ion etching. The whole device is transferred to the PDMS spin coated on the polyvinyl alcohol and encapsulated by another PDMS via spin coating. To attach devices to target substrates (for example, prosthetic hand), the encapsulated device is attached on the target position and then the polyvinyl alcohol film is removed through immersion in DI water.

6.2 Measurement of skin-segment deformations with motion capturing system

A motion capture system is used to measure regional stretchability of skin in the hand and knee regions during various movements. Thirty-one reflective markers (diameter: 3 mm) are attached with ~1.5 cm inter-spacing. The locations and angles of the twelve motion capture cameras (OptiTrack Prime 41, NaturalPoint, USA) are adjusted to

optimize signal to noise during the calibration process. The subject wearing reflective markers systematically moves his limbs and motion capture cameras record positional changes of each reflective marker. The recorded data are then analyzed with motion tracking software (Motionbuilder, Autodesk, USA). The amount of skin stretch is estimated by calculating distance changes between nearby reflective markers

6.3 Finite element analysis (FEA) of strain gauges

Finite element simulations are used to analyze the strain distribution of SiNR strain gauges during stretching tests. The SiNR strain gauges with different serpentine designs are modeled using four-node composite shell elements. The strain gauges are embedded between two 60 μm -thick PDMS substrates which are modeled using eight-node solid elements. I assume perfect bonding (no slip condition) between sensors and PDMS substrates. Linear elasticity represents the behavior of the sensor materials. The following anisotropic elasticity parameters are used for single crystalline silicon: $E_{xx} = E_{yy} = 169$ GPa, $\nu_{xy} = 0.064$, $G_{xy} = 50.9$ GPa, $G_{xz} = G_{yz} = 79.6$ GPa, where E and ν denote the Young's modulus and the Poisson's ratio, respectively. The x - and y - axes in Fig. 3a are the $\langle 110 \rangle$ directions. The Young's moduli of gold, chromium, and PI are 77.2 GPa, 279 GPa, and 2.5 GPa, respectively. The Poisson's ratios of gold, chromium, and PI are 0.42, 0.21, and 0.34, respectively. The incompressible neo-Hookean model is used to represent the PDMS substrate:

$$W = C_1(I_1 - 3)$$

where W is the strain energy potential, I_1 is the first invariant of the left Cauchy-Green tensor, and C_1 (=18 kPa for PDMS) is a material parameter.

6.4 Strain mapping using a multiplexer/matrix switch

To measure the resistance changes of dozens of strain gauges/pressure sensors, I use two source measurement units (SMUs; NI PXIe-4143, National Instruments, USA) that have four channels each and a 128-channel multiplexer/matrix switch (NI PXI-2530B, National Instruments, USA). By using the multiplexer switch, resistances of SiNR strain gauge/pressure sensor arrays are measured sequentially to map regional strain/pressure changes. Six neighboring strain/pressure sensors are grouped and averaged. The complete map of the strain/pressure distribution is obtained by interpolating averaged data over the entire sensing area by using MATLAB software (Mathworks, USA).

6.5 Surgical procedures to expose sciatic nerves of rat

A Sprague Dawley rat is anesthetized by intraperitoneal injection of ketamine (100 mg/kg) and xylazine hydrochloride (5 mg/kg). During the induction of anesthesia, the rat is kept at room temperature, shaved near the buttock area, and placed in prone position. After the skin incision, the gluteus muscles are exposed and dissected until the sciatic nerve is visible.

6.6 Measurement of Electroencephalography signals from rat's brain

To simultaneously measure the electrophysiological signals from the rat's brain, electrode implantation is performed with a stereotaxic apparatus (Kopf Instruments). Evoked potential recordings are obtained with stainless steel electrodes (0.005 in, Plastics One), positioned in ventral posterolateral nucleus (VPL) of the thalamus (AP: -2.3 mm, ML: 3.0 mm, and DV: -6.0 to -7.0 mm) in the right hemisphere. A reference electrode is inserted on the skull above the cerebellum. The electrodes are fixed to the skull with cyanoacrylate adhesive and dental acrylic cement. The neural activity is recorded after the signals are amplified 1200-fold, band pass-filtered at 0.1-100 Hz, and digitized at a sampling rate of 400 Hz using a digital EEG system (Comet XL, Astro-Med, West Warwick, RI, USA).

6.7 Synthesis of PtNWs on Au electrode

H_2PtCl_6 ($\geq 99.5\%$, Sigma Aldrich) solution of 1% (w/w) containing 1.5 M HClO_4 (70%, ACS reagent, Sigma Aldrich) are prepared for the electrodeposition. A porous AAO template (Anodisc, Whatman) is laminated onto Au electrode array and dipped into the H_2PtCl_6 solution. A custom made holder firmly fixes the AAO template on Au electrodes. Electrodeposition is performed by using the electrochemical workstation with the three-electrode system: a platinum, Ag/AgCl and Au electrode as a counter, reference and

working electrode. Using potentiostatic mode with the potential of -0.35V, electrodeposition is carried out for ~30 min at the room temperature. After the deposition is completed, the sample is washed with the triple-distilled water. Finally it is immersed into 1M NaOH solution at room temperature for ~30 min to dissolve the AAO template.

6.8 Synthesis of ceria nanoparticles

1 mmol (0.4 g) of cerium (III) acetate (98%, Sigma- Aldrich) and 12 mmol (3.2 g) of oleylamine (approximate C18-content of 80–90%, AcrosOrganics) are added to 15 mL xylene (98.5%, Sigma-Aldrich). The mixed solution is treated by the sonicator for ~15 min at room temperature and then heated to 90 °C. 1 mL of deionized water is injected into the solution under vigorous stirring at 90 °C, and then the solution color changes to an off-white color, representing that the reaction had occurred. The resulting mixture is aged at 90 °C for 3 h to give a light yellow colloidal solution, which is then cooled to room temperature. Acetone (100 mL) is added to the precipitated ceria nanoparticles. The precipitate is washed with acetone using centrifugation and the resulting ceria nanoparticles are easily dispersible in chloroform.

6.9 Anti-oxidant properties of ceria nanoparticles

To verify anti-oxidant properties of ceria nanoparticles, catalase mimetic assay is used. Quenching hydrogen peroxide is quantified using Amplex[®] Red Hydrogen Peroxide/Peroxidase assay kit (Molecular Probes Inc.). Amplex Red reagent (10-acetyl-3,7-dihydroxyphenoxazine) reacts with H₂O₂ and it produces the red fluorescent resorufin

with the horseradish peroxide (HRP). The fluorescence of resorufin (excitation at 571 nm and emission at 585 nm) indicates the H_2O_2 levels in the samples. First, the H_2O_2 standard curve is prepared for determining H_2O_2 concentration in each sample. After drop casting 30 μL of 5 mM ceria nanoparticle solutions on the PtNWs-decorated electrodes, each sample is placed in each micro well and 50 μL of H_2O_2 solutions are added. 50 μL of the Amplex[®] Red reagent/HRP working solution is subsequently added. The initial concentration of H_2O_2 is 5 μM . The fluorescence is measured after incubating for 30 min at room temperature.

7. Conclusion

In this paper, the stretchable and multi-functional sensors on artificial skin are shown. Based on motion-capture videography analysis, maps of skin deformation in response to various motions are acquired and this information form the site-specific geometries and design for SiNR-based devices. With site-specifically designed SiNR, mechanical and tactile sensors exhibit wide detection ranges and enhanced mechanical durability. Ultrathin structure and neutral mechanical plane configurations also produce mechanical stability under various deformations. Co-integrated humidity sensors and heaters made the proposed artificial skin more realistic by providing humidity sensing and body temperature emulating capabilities. Interfacing stretchable MEA decorated with PtNWs and ceria nanoparticles show the capability of biointegration with nervous system. Therefore, sensing and actuation capabilities are achieved in prosthetic device through artificial skin with enhanced sensing ranges.

8. References

1. Dahiya, R. S. & Valle, M. *Robotic tactile sensing* Ch. 3 (Springer Science+Business Media, Dordrecht, 2013).
2. Tabot, G. A. *et al.* Restoring the sense of touch with a prosthetic hand through a brain interface. *Proc. Natl. Acad. Sci. USA.* **110**, 18279-18284 (2013).
3. Raspopovic, S. *et al.* Restoring natural sensory feedback in real-time bidirectional hand prostheses. *Sci. Transl. Med.* **6**, 222ra19 (2014).
4. Tan, D. W. *et al.* A neural interface long-term stable natural touch perception. *Sci. Transl. Med* **6**, 257ra138 (2014).
5. Dilton, G. S. *et al.* Direct neural sensory feedback and control of a prosthetic arm. *IEEE. T. Neur. Sys. Reh.* **4**, 468-472
6. Graz, I. *et al.* Flexible active-matrix cells with selectively poled bifunctional polymer-ceramic nanocomposite for pressure and temperature sensing skin. *J. Appl. Phys.* **106**, 034503 (2009).
7. Mannsfeld, S. C. B. *et al.* Highly sensitive flexible pressure sensors with microstructured rubber dielectric layers. *Nature Mater.* **9**, 859-864 (2010).
8. Lipomi, D. J. *et al.* Skin-like pressure and strain sensors based on transparent elastic films of carbon nanotubes. *Nature Nanotech.* **6**, 788-792 (2011).
9. Pang, C. *et al.* A flexible and highly sensitive strain-gauge sensor using reversible interlocking of nanofibres. *Nature Mater.* **11**, 795-801 (2012).
10. Persano, L. *et al.* High performance piezoelectric devices based on aligned

- arrays of nanofibers of poly(vinylidene fluoride-co-trifluoroethylene). *Nature Commun.* **4**, 1633 (2013).
11. Vandeparre, H., Watson, D. & Lacour, S. P. Extremely robust and conformable capacitive pressure sensors based on flexible polyurethane foams and stretchable metallization. *Appl. Phys. Lett.* **103**, 204103 (2013).
 12. Kim, D.-H. *et al.* Epidermal electronics. *Science* **333**, 838-843 (2011).
 13. Lu, N., Lu, C., Yang, S. & Rogers, J. Highly sensitive skin-mountable strain gauges based entirely on elastomers. *Adv. Funct. Mater.* **22**, 4044-4050 (2012).
 14. Jung, S. *et al.* Reverse-micelle-induced porous pressure-sensitive rubber for wearable human-machine interfaces. *Adv. Mater.* **26**, 4825-4830 (2014).
 15. Someya, T. *et al.* Conformable, flexible, large-area networks of pressure and thermal sensors with organic transistor active matrixes. *Proc. Natl. Acad. Sci. USA* **102**, 12321-12325 (2005).
 16. Sekitani, T. *et al.* Organic nonvolatile memory transistors for flexible sensor arrays. *Science* **326**, 1516-1519 (2009).
 17. Sekitani, T., Zschieschang, U., Klauk, H. & Someya, T. Flexible organic transistors and circuits with extreme bending stability. *Nature Mater.* **9**, 1015-1022 (2010).
 18. Kaltenbrunner, M. *et al.* An ultra-lightweight design for imperceptible plastic electronics. *Nature* **499**, 458-463 (2013).
 19. Takei, K. *et al.* Nanowire active-matrix circuitry for low-voltage macroscale artificial skin. *Nature Mater.* **9**, 821-826 (2010).

20. Wang, C. *et al.* User-interactive electronic skin for instantaneous pressure visualization. *Nature Mater.* **12**, 899-904 (2013).
21. Son, D. *et al.* Multifunctional wearable devices for diagnosis and therapy of movement disorders. *Nature Nanotech.* **9**, 397-404 (2014).
22. Ying, M. *et al.* Silicon nanomembranes for fingertip electronics. *Nanotechnology* **23**, 344004 (2012).
23. Webb, R. C. *et al.* Ultrathin conformal devices for precise and continuous thermal characterization of human skin. *Nature Mater.* **12**, 938-944 (2013).
24. Li, X. *et al.* Measurement for fracture toughness of single crystal silicon film with tensile test. *Sensor Actuat A-Phys.* **119**, 229-235 (2005).
25. Suo, Z. Mechanics of stretchable electronics and soft machines. *MRS Bulletin* **37**, 218-225 (2012).
26. Ackerley, R., Olausson, H., Wessberg, J. & McGlone, F. Wetness perception across body sites. *Neurosci. Lett.* **522**, 73-77 (2012).
27. Fan, J. A. *et al.* Fractal design concepts for stretchable electronics. *Nature Commun.* **5**, 3266 (2014).
28. Spira, M. E. & Hai, A. Multi-electrode array technologies for neuroscience and cardiology. *Nature Nanotech.* **8**, 83-94 (2013).
29. Viventi, J. *et al.* Flexible, foldable, actively multiplexed, high-density electrode array for mapping brain activity *in vivo*. *Nature Neurosci.* **14**, 1599-1605 (2011).
30. Grill, W. M., Norman, S. E. & Bellamkonda, R. V. Implanted neural interfaces: biochallenges and engineered solutions. *Annu. Rev. Biomed. Eng.* **11**, 1-24 (2009).

31. Kim, C. K. *et al.* Ceria nanoparticles that can protect against ischemic stroke. *Angew. Chem. -Int. Edit.* **51**, 11039-11043 (2012).
32. Lacour S. P. *et al.* Flexible and stretchable micro-electrodes for in vitro and in vivo neural interfaces. *Med. Biol. Eng. Comput.* **48**, 945-954 (2010).
33. Jeon, D. *et al.* Observational fear learning involves affective pain system and Cav 1.2 Ca²⁺ channels in ACC. *Nature Neurosci.* **13**, 482-488 (2010).
34. Khalid, A. *et al.* Tracing the evolution of multi-scale functional networks in a mouse model of depression using persistent brain network homology. *NeuroImage* **101**, 351-363.

위치 특이적으로 고안된 실리콘 나노리본 기반의 장치를 이용한 다기능성 전자피부

서울대학교 대학원

협동과정 바이오엔지니어링

이민철

의수 등의 보철기기 기술의 발전으로 인해 화상이나 당뇨, 전쟁 등의 사고에 의해 팔 또는 다리를 잃은 절단환자들이 보철기기를 통해 신체 움직임을 대신할 수 있는 일이 더이상은 불가능한 일이 아닌 상황이 되었다. 보철기기의 움직임을 실제 팔다리와 유사하게 세밀하게 구동시키기 위해서는 의수로부터 인체로 전달되는 감각 피드백이 필요하다. 이뿐만 아니라 기존 상용화에 가까운 보철 기술은 움직임을 제공하여 유실된 신체의 운동능력을 제공하지만 감각능력은 복구할 수 없는 상황이기 때문에, 보철기기에서 외부 자극을 감지할 수 있는 감각능력과 그 감지된 신호를 신체로 전달할 수 있는 피드백에 관한 연구는 더욱 필요하다. 이와 같은 필요성을 충족시키기 위해 전자피부를 이용해 보철기기 혹은 피부 위에서 외부 자극에 대한 감지 능력을 구현하기

위한 연구들이 많이 이루어졌다. 하지만 기존의 연구들에서는 실제 피부와 같이 탄력성이 있으면서도 시공간적 해상도가 높고, 물리적 자극에 대한 내구도가 높은 특성을 모사하기가 힘들었다. 따라서 이번 연구에서는 신축성이 있으면서도 여러가지 자극에 대한 감지능력 (피부변형, 압력, 습도)을 지는 전자 피부를 구현하였다. 특히, 단결정의 실리콘 나노리본을 실제 의수의 움직임에 따른 변형을 고려하여 의수 위 위치에 따라 다른 디자인을 갖도록 하였고, 이를 통해 큰 변형 범위에서도 안정적으로 감지능력을 유지할 수 있도록 하였다. 이뿐만 아니라 세리아 나노파티클이 코팅된 백금 나노 와이어가 결합된 신축성 있는 전극을 이용하여 전자피부에서 획득한 신호를 신경계에 전달할 수 있는 피드백 시스템을 동물 실험을 통해 구현하였다. 신축성 있는 디자인과 세리아 나노파티클은 인체 삽입시 발생할 수 있는 면역반응을 고려하여 고안되었다. 이 같이 외부 자극에 대한 감지능력과 그 신호를 신경계로 전달할 수 있는 시스템은 유실된 인체 기능 복구를 위한 보철 기술에 효과적인 대책이 될 것이다.

주요어 : 신축성 있는 전자소자, 유연 전자소자, 전자 피부, 생체신호 측정

학번 : 2013-23195